# Probing new charged scalars with neutrino trident production

Gabriel Magill* and Ryan Plestid†

*Department of Physics and Astronomy, McMaster University, Hamilton, Ontario, Canada and Perimeter Institute for Theoretical Physics, Waterloo, Ontario, Canada*

(Received 20 November 2017; published 5 March 2018)

We investigate the possibility of using neutrino trident production to probe leptophilic charged scalars at future high intensity neutrino experiments. We show that under specific assumptions, this production process can provide competitive sensitivity for generic charged scalars as compared to common existing bounds. We also investigate how the recently proposed mixed-flavor production—where the two oppositely charged leptons in the final state need not be muon flavored—can give a 20%–50% increase in sensitivity for certain configurations of new physics couplings as compared to traditional trident modes. We then categorize all renormalizable leptophilic scalar extensions based on their representation under $\mathrm{SU}(2) \times \mathrm{U}(1)$, and discuss the Higgs triplet and Zee-Babu models as explicit UV realizations. We find that the inclusion of additional doubly charged scalars and the need to reproduce neutrino masses make trident production uncompetitive with current bounds for these specific UV completions. Our work represents the first application of neutrino trident production to study charged scalars. Additionally, it is the first application of mixed-flavor trident production to study physics beyond the standard model more generally.

DOI: 10.1103/PhysRevD.97.055003

## I. INTRODUCTION AND MOTIVATION

Neutrino oscillation experiments provide conclusive evidence that the standard model (SM) is incomplete. Many unresolved anomalies—the proton radius puzzle [1,2], the anomalous magnetic moment of the muon [3,4], and the Liquid Scintillator Neutrino Detector anomaly [5]—can be interpreted as providing hints into beyond the SM (BSM) physics, especially for heavy leptons where constraints are typically weaker. Scalar extensions of the SM have been proposed as solutions to all of these anomalous measurements [6–9]. Currently, most constraints on the scalar sector come from low energy observables and high energy colliders [10,11]. In contrast, high intensity mid energy neutrino experiments have remained relatively uninvestigated. Consequently, new tools sensitive to interactions between scalars and neutrinos/heavy leptons provide a complimentary probe of BSM physics.

Neutrino trident production (NTP) represents a natural candidate for studying couplings to an extended scalar sector given the successful application of NTP to models with an Abelian $Z'$ coupled to $L_\mu - L_\tau$ [12]. Using data from the beam dump experiments CHARM-II and CCFR [13,14] the authors of Ref. [12] were able to probe previously unexplored parameter space, including part of the favored region for the resolution of the $(g-2)_\mu$ anomaly. As demonstrated in Ref. [15], the upcoming beam dump experiments SHiP and DUNE [16,17] are sensitive to many previously unmeasured neutrino trident channels which contain mixed-flavor leptons in the final state. With these exciting new prospects the possibility of NTP serving as a powerful probe of scalar extensions seems highly probable. Furthermore, given the mounting interest in precision neutrino physics, NTP may find applications at other future neutrino experiments, in particular, Fermilab's short-baseline neutrino program [18].

NTP involves the creation of a lepton pair via a high energy neutrino scattering coherently (diffractively) with a nucleus (nucleon) as shown in Fig. 1. This production mechanism is subdominant to charged-current (CC) scattering, in large part due to the extra $\alpha^2$ fine-structure suppression in its cross section; for 50 GeV neutrinos scattering coherently on lead producing a $\mu^+\mu^-$ final state, we expect one trident event for every $10^5$ CC events [19]. As discussed in Ref. [15], this scaling depends largely on the flavors of the final state lepton pair, with event rates being 40 times larger in the case of $e^+\mu^-$ production at DUNE. This is due to the absence of W-Z interference, and an infrared singularity in the phase space; the lower electron mass provides a log-enhanced cross section.

*gmagill@perimeterinstitute.ca
†plestird@mcmaster.ca

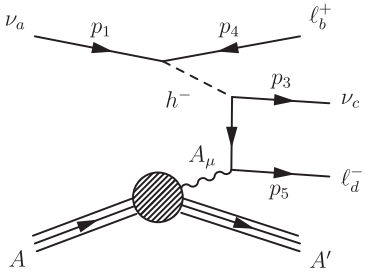


FIG. 1. Neutrino trident production of a charged Weyl lepton pair via a new charged scalar. There are three additional diagrams that can be obtained. The two charged leptons can be of different flavors. The connecting photon can interact with the nucleus (as shown above), or with individual nucleons.

Multiflavor configurations were not observable in CCFR or CHARM-II due to difficulties in tagging electron final states. The potential to view these NTP processes at future experiments allows for a rich landscape of signals [15,20,21]. In particular, it lends itself to the study of off-diagonal lepton flavor couplings, and these appear naturally for new charged scalars. In this work, we study how these new mixed-flavor observables compare with existing probes of charged scalar theories that preserve the SM's $\mathrm{SU}(2)\times\mathrm{U}(1)$; we assume no additional fermion or vector content. The case of neutral scalars probed via the diagonal $\nu\mu^+\mu^-$ final state has been considered for a phenomenologically motivated Lagrangian in Ref. [22].

We find that charged scalars are best probed by NTP in the case of universal flavor diagonal couplings. For these configurations, we find that mixed-flavor trident final states can give a 20%–50% increase in sensitivity to BSM couplings as compared to the traditional $\nu\mu^+\mu^-$-trident channel, and consequently outperforming bounds from the anomalous magnetic moment of the muon. When considering explicit UV completions (such as a Higgs triplet), we characterize the experimental improvements one should make in order for bounds from NTP to be competitive. Additional neutral and doubly charged scalar particles often appear in the context of UV models reproducing neutrino oscillation data, and these can introduce new, and more stringent, constraints.

The rest of the article is organized as follows: In Sec. II, we consider a general leptophilic charged scalar, how it contributes to trident, and its associated experimental backgrounds. For some benchmark choices in parameter space, we show the reach in sensitivity. In Sec. III, we explain how our general model can arise by giving an exhaustive classification of all leptophilic, renormalizable and $\mathrm{SU}(2)\times\mathrm{U}(1)$ invariant scalar extensions. We discuss specific realizations of these classifications in the literature and in Sec. IV, the phenomenological constraints surrounding them. We conclude with general remarks and potential applications in Sec. V.

## II. CHARGED SCALAR MEDIATED TRIDENT PRODUCTION

### A. Signal

We consider a singly electrically charged scalar $h$ coupling to the lepton doublets,

$$\mathcal{L}\supset|\partial_\mu h|^2+|\partial_\mu k|^2-m_h^2|h|^2+\sqrt{2}h_{ab}\nu^a\ell^b h + k_{ab}\ell^a\ell^b k+\text{c.c.} \tag{1}$$

The doubly electrically charged scalar $k$, which does not contribute to NTP, has been included to make connection with UV completions. The singly charged scalar contributes to NTP via diagrams like the one shown in Fig. 1 and results in the amplitude shown in Eq. (2). In the following, we use $x^\alpha$ and $y^\dagger_\alpha$ to denote left- and right-handed initial states respectively, and $y^\alpha$ and $x^\dagger_\alpha$ to denote right- and left-handed final states, following [23]. We assign the labels $\{1,2,3,4,5\}=\{\nu,\gamma,\nu',\ell^+,\ell^-\}$, and we use the mostly minus metric $\eta_{\mu\nu}=\{1,-1,-1,-1\}$.

In the context of the equivalent photon approximation [19,24], the matrix element for $\gamma\nu_a\to\ell_b^+\nu_c\ell_d^-$ can be summarized succinctly as

$$\begin{aligned}\mathcal{M}_h&=-\frac{2h_{ab}h^*_{cd}e}{(P_1-P_4)^2-m_h^2}\left[\frac{\mathcal{A}_{14}}{q_d^2-m_d^2}+\frac{\mathcal{A}_{35}}{q_b^2-m_b^2}\right]\\ \mathcal{A}_{14}&=\{(x_1y_4)(x_3^\dagger\bar{\not{q}}_d\not{\ell}_2x_5^\dagger)+(x_1y_4)(x_3^\dagger\bar{\not{\ell}}_2y_5)m_d\}\\ \mathcal{A}_{35}&=\{(x_1\not{q}_b\bar{\not{\ell}}_2y_4)(x_3^\dagger x_5^\dagger)+(x_1\not{\ell}_2x_4^\dagger)(x_3^\dagger x_5^\dagger)m_b\}\\ q_b&\equiv P_2-P_4\quad q_d\equiv P_2-P_5\quad \not{\ell}=\ell\cdot\sigma\quad \bar{\not{\ell}}=\ell\cdot\bar{\sigma},\end{aligned} \tag{2}$$

where $\{a,b,c,d\}$ label lepton generations.

The above matrix element contains contributions from four different diagrams. Two contain mass insertions appearing in the second terms of $\mathcal{A}_{14}$ and $\mathcal{A}_{35}$. The two amplitudes correspond to the photon interacting with either the negatively or positively charged lepton. The following identities,

$$u=(x,y^\dagger)^T\quad v=(y,x^\dagger)^T\quad \bar{u}=(y,x^\dagger)\quad \bar{v}=(x,y^\dagger), \tag{3}$$

can be used to rewrite the amplitudes in terms of the Dirac spinors,

$$\begin{aligned}\mathcal{A}_{14}&=\bar{v}_1P_Lv_4\bar{u}_3P_R(\not{q}_d+m_d)\not{\ell}_2v_5,\\ \mathcal{A}_{35}&=\bar{v}_1P_L(\not{q}_b+m_b)\not{\ell}_2v_4\bar{u}_3P_Rv_5.\end{aligned} \tag{4}$$

As a check of our calculations, we used the symbolic manipulation language FORM [25] and compared our results to [20]. LEP searches rule out charged Higgs for $m_{h^\pm}\lesssim 100$ GeV on general grounds based solely on its electromagnetic interactions with the photon and $Z$ boson

[26] and so we have ignored the four-momentum in the scalar's propagator. The full cross section is obtained from Eq. (2) by

$$\sigma_{N\nu} = \frac{Z^2\alpha}{\pi}\int_{m_{jk}^2}^{S}\frac{\mathrm{d}s}{s}\sigma_{\gamma\nu}(s)\int_{(s/2E_\nu)^2}^{\infty}\frac{\mathrm{d}Q^2}{Q^2}F^2(Q^2), \quad (5)$$

where $F(Q^2)$ above is the Woods-Saxon form factor [15,27].

For generic NTP final states the SM and BSM contributions can both be treated as real. The sign of the interference is dictated by the symmetry or antisymmetry of the couplings in Eq. (2), as well as the relative sign of the SM contribution. For a given NTP process, the presence of $Z$ and/or $W$ vector mediators induces an axial ($C_A$) and vector ($C_V$) coupling, upon which the matrix element depends linearly [15]. If the SM mediators are both $W$ and $Z$ bosons ($C_{V,A} > 0$), we find a positive relative sign. When the mediator is only a $Z$ boson ($C_{V,A} < 0$), we get a negative sign. When the mediator is only a $W$ boson ($C_{V,A} = 1$), we find a positive sign for $m_+ > m_-$ and a negative one when $m_+ < m_-$; this effect is related to subtle helicity properties [15]. For antisymmetric couplings $h_{e\mu} = -h_{\mu e}$ the new physics part of the matrix element carries an additional negative sign, while for the symmetric case ($h_{e\mu} = h_{\mu e}$), there is a positive sign. The final results for the sign of the interference terms are shown in Appendix C. For symmetric (antisymmetric) couplings, we have mostly constructive (destructive) interference.

### B. Search strategy and backgrounds

Many flavor combinations for the incoming neutrino, outgoing neutrino, and charged leptons are possible. In deciding which reaction channel is ideally suited to one's purposes, two strategies should be considered. First, a channel with a relatively high SM contribution could be chosen, allowing for interference effects, which will be dominant in the limit of small coupling.[1] Neutrino beams are predominantly composed of $\nu_\mu$ and so, in considering interference-driven signals, we typically consider incident $\nu_\mu$. Phase space considerations cause NTP rates to favor lighter lepton masses [15] and so we focus our analysis on final states with at least one electron, or positron. When considering the older experiments CCFR and CHARM-II we consider their reported observations of $\mu^+\mu^-$ production.

A complementary approach is to consider a production channel that is closed in the SM, but open in the case of new physics. To ensure low backgrounds, one needs to be able to control the flux of incident (anti)neutrinos. To see this consider $\nu_\mu \to e^-\mu^+\nu$ which is SM forbidden, but possible in the presence of BSM scalars. If, however, the beam was contaminated with $\bar{\nu}_\mu$, then the SM allowed $\bar{\nu}_\mu \to \mu^+ e^- \bar{\nu}_e$ would present a substantial background. DUNE has the capability to eliminate contamination with its neutrino horn. In contrast, SHiP has a much more complicated incident flux profile and cannot separate the neutrino and antineutrino fluxes.

The sensitivities we present in this paper are based on future experiments measuring rates consistent with the irreducible SM coherent NTP backgrounds. The details of the procedure are outlined in Appendix C, and numerical sensitivity equations are shown in Tables III and IV. A full simulation would have to be performed by the collaborations prior to their analysis, but we believe our analysis provides a good approximation. For simplicity, we focus the discussion on SHiP; however DUNE is also well equipped to tackle the same backgrounds.

The SHiP tau neutrino detector, modeled after the OPERA experiment [29], is based on emulsion cloud chambers (ECC) technology. The ECC is composed of a series of thin films interleaved with lead plates, followed by a muon spectrometer. A qualitatively similar setup to this was used in the CCFR experiment [14,30], which featured iron plates interleaved with liquid scintillators and drift chambers. The use of fine emulsion film layers will provide SHiP with more accurate track ID capabilities as compared to CCFR. That said, CCFR was able to observe a $\mu^+\mu^-$-trident rate of 37 events given a theoretical SM prediction of 45 events. They isolated their signal by collecting $\mu^-$ and $\mu^+$ events and imposing cuts on the energy, angles, total invariant mass, hadronic activity, and vertex resolution. SHiP can implement similar cuts; however one caveat is that CCFR was dealing with much larger incoming neutrino average energies (∼160 GeV) as compared with SHiP and DUNE providing it with an enhanced signal [15,19]. Since the bulk of these trident events are expected to come from SM processes, the kinematics of the outgoing pair of charged leptons is well captured in [20,21].

Consider a mixed-flavor $\ell_b^+\ell_d^-$ lepton pair search with a hadronic veto. Final $e^+e^-$ states can arise from resonant $\pi^0$ production followed by a Dalitz decay where one of the photons is lost. For $\mu^-\mu^+$ final states, the dominant backgrounds are from $\nu_\mu A \to \mu^- YX$, where $Y$ represents either a pion, kaon, charm- or $D$-meson which decays to a final state involving $\mu^+$ [31], as seen by NuTeV. Production of vector meson final states is also likely, but these can be distinguished from NTP since they deposit more hadronic energy and lead to a larger invariant mass for the lepton pair. The decay length of pions is on the order of a few meters, and therefore these backgrounds could also contribute to $\mu^- e^+$ mixed-flavor final states if the meson fakes a charged lepton before decaying. The fake rate suppression at SHiP is very competitive. In particular, for electron ID efficiencies greater than 80%, the pion contamination rate is roughly $\eta_{\pi\to e} \leq 0.5\%$ [32]. In the SHiP detector at

[1]This interference is not sensitive to the phases of the couplings, which can be expected on general grounds related to the arbitrary definitions of phases in $h_{ab}$ [28].

the end of the decay chamber, pion contaminations of $\eta_{\pi\to\mu} = 0.1\%$ can be achieved for muon identification efficiencies of roughly 1. For $e^-$ and $\mu^+$ final states, it is difficult to imagine how this would be produced outside of NTP. One possibility is coherent pion production from a $\bar{\nu}_e$ incoming state and a negatively charged pion. This background is expected to be small for a number of reasons, owing to the differences in the $\ell^+$ and $\ell^-$ energy spectrum, the much smaller lifetime flux of $\bar{\nu}_e$ at SHiP. Combinatorial backgrounds where one observes an electron and an antimuon from two unrelated processes could be eliminated by the micron vertex resolution available at both SHiP and DUNE.

### C. Model independent results

In this section, we illustrate the sensitivity of mixed-flavor NTP to charged scalars. We also highlight how certain flavor configurations precluded in the SM give superior sensitivity to existing constraints. As an illustrative example, we consider the model described by Eq. (1) and assume that $h_{aa} = |h|$, and $h_{ab} = 0$ for $a \neq b$. As is eventually discussed in Appendix B, most of the strong existing constraints commonly considered for these types of models [10,11] drop out and NTP provides the dominant constraint, outperforming the $(g-2)$ for the muon. Our results are shown in Fig. 2.

We have forecasted the SM backgrounds at SHiP and DUNE using the rates presented in [15]. The best performing mode is the $\mu^+e^-$ channel at DUNE. *A priori*, the irreducible backgrounds to this process are $\bar{\nu}_\mu \to \mu^+\bar{\nu}_e e^-$ and $\nu_e \to \mu^+\nu_\mu e^-$. However, DUNE will have the ability to run in neutrino and antineutrino mode independently. This, coupled to the fact that the $\nu_e$ luminosities are low at this experiment, makes this channel a 0 irreducible background search. Hence, we can use this channel to investigate the interplay between 0 background and the lack of interference term in the cross section. We make the interesting

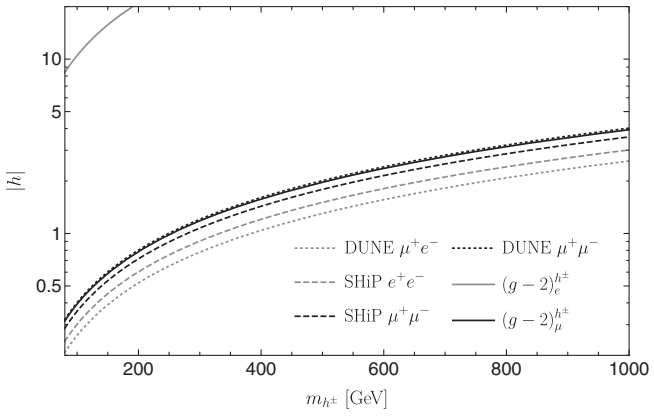


FIG. 2. Projected 90% C.L. sensitivities at DUNE and SHiP for a given pair of final state oppositely charged leptons, and competing constraints when allowing only $h_{ee} = h_{\mu\mu} = h_{\tau\tau} \neq 0$.

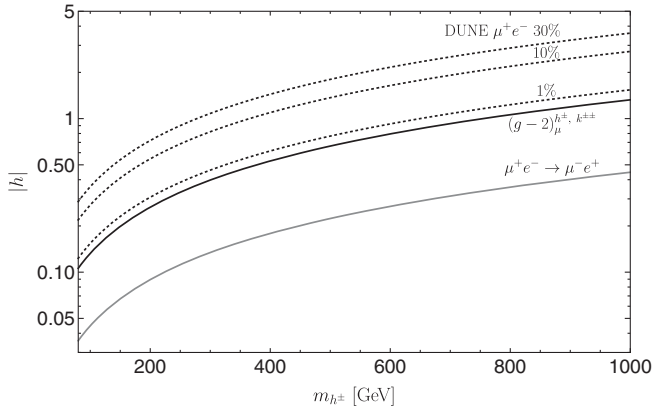


FIG. 3. Projected sensitivities of NTP assuming the SM prediction at DUNE has been measured to various precisions measured as a percentage of the SM cross section. We compare this to other constraints which now include a doubly charged scalar.

observation that the mixed-flavor final states in both experiments provide stronger constraints than the $\mu^+\mu^-$ states, while probing a Yukawa diagonal theory. In going from the muon final states to more general final states, the sensitivities to $|h|$ at DUNE are improved by 50% whereas at SHiP, they can be improved up to 20%.

We now show how NTP compares to other constraints when taking into account doubly charged scalars, assuming that $h_{ab} = k_{ab}$ in Eq. (2). This is analogous to the Higgs triplet (HT) model to be discussed later, without imposing the requirements of reproducing neutrino masses. The introduction of a doubly charged scalar $k^{\pm\pm}$ implies additional constraints from $\mu^+e^- \to \mu^-e^+$. A natural question to ask is the following: What improvements in sensitivity are required to make trident competitive with these stronger constraints? We assume that one could measure the NTP cross section to within a given percentage of the SM cross section, for various benchmark precisions. These results are presented in Fig. 3. As a reference, the 10% curve for DUNE's $\mu^+e^-$ channel corresponds roughly to the 90% C.L. bounds shown in Fig. 2. As can be seen, very high precision in the measured NTP cross section would be required to compete with the leading constraints on scalar couplings assuming $k^{\pm\pm}$.

## III. EXTENSIONS ABOVE THE ELECTROWEAK SCALE

We now illustrate how the phenomenological charged scalar model from Sec. II can minimally arise while obeying all of the symmetries of the SM, with no additional fermion or vector matter content. The lepton sector's $SU(2) \times U(1)$ structure restricts possible scalar couplings that are relevant for NTP. The relevant leptonic fields are the SU(2) doublets and singlets denoted by

TABLE I. Classification of renormalizable lepton-scalar operators consistent with gauge invariance. The final column denotes the flavor symmetry ($\{ab\}$) or antisymmetry ($[ab]$) due to the SU(2) structure.

| Field | U(1) | SU(2) | $\mathcal{L}_{\text{int}}$ | Couplings |
|---|---|---|---|---|
| $\mathcal{S}$ | $-2$ | 1 | $\mathcal{S}\ell^c_a\ell^c_b$ | $s_{\{ab\}}$ |
| $\mathcal{F}$ | 1 | 1 | $\mathcal{F}\epsilon_{ij}L^{[i}_a L^{j]}_b$ | $f_{[ab]}$ |
| $\mathcal{D}$ | $-\frac{1}{2}$ | 2 | $\mathcal{D}_i L^i_a \ell^c_b$ | $d_{ab}$ |
| $\mathcal{T}$ | 1 | 3 | $\mathcal{T}_{\{ij\}}L^{\{i}_a L^{j\}}_b$ | $t_{\{ab\}}$ |

$$L^i_a = \begin{pmatrix} \nu_a \\ \ell_a \end{pmatrix}, \qquad \ell^c_a \tag{6}$$

respectively, where $i$ labels the SU(2) index, and $a \in \{e,\mu,\tau\}$ labels the generations. All fields above are two-component left-handed spinors, with the spinor indices suppressed [i.e. $\ell^c_a = (\ell^c_a)_\alpha$]. To couple these fermions to a scalar via a renormalizable interaction we can consider at most two lepton fields and one scalar. The possibilities are given in Table I, where the lowercase letters represent generational coupling matrices, and the capital script letters are the scalar fields. In the order shown in the table, these are the symmetric singlet, antisymmetric singlet, doublet, and triplet models. The $s_{ab}$ and $t_{ab}$ couplings are symmetric in their indices. As for $f_{ab}$, the antisymmetry under the $i \leftrightarrow j$ forces $f_{ab}$ to be antisymmetric under $a \leftrightarrow b$. The couplings for $d_{ab}$ are unconstrained. A doubly charged scalar such as $S$ cannot contribute to NTP at tree level, and we therefore focus on the fields $\mathcal{F}$, $\mathcal{D}$, and $\mathcal{T}$ for the purposes of NTP. The primary effects of the SU(2) symmetry are to

(i) Enforce a relation between couplings of the neutral, singly, and doubly charged scalars. This occurs for the triplet case and introduces additional constraints with which NTP must compete.
(ii) Generate flavor symmetries in the couplings which can lead to constructive or destructive interference.

To discuss specific implementations of the $\mathcal{D}$, $\mathcal{T}$ and $\mathcal{F}$ classifications, we respectively consider the Two-Higgs-doublet model, the HT model (also known as type-II seesaw), and the Zee-Babu (ZB) model. The full details of these models [10,11,28,33] are discussed in Appendix A. Here, we summarize the important features of the latter two theories. HT and ZB models both generate neutrino masses and feature a doubly charged scalar. In the ZB model, the couplings of leptons to the singly charged and doubly charged scalars are allowed to vary independently, whereas in the HT model, they are identical. In order to preserve the $\mathrm{SU}(2)\times\mathrm{U}(1)$ structure of the SM, the HT model contains in addition a neutral scalar which only couples to neutrinos. Without any extra model building, the neutral scalars considered in this paper cannot contribute to NTP in contrast to the models considered in Ref. [22]. To help make the connection with Sec. II, we show important coupling relations in Table II.

TABLE II. Relationships between type-II seesaw, Zee-Babu, and generic couplings $h_{ab}$ and $k_{ab}$. Curly (square) braces mark the couplings' (anti)symmetry.

| Scalar extension | $\sqrt{2}h_{ab}$ | $h^\pm$ | $k_{ab}$ | $k^{\pm\pm}$ |
|---|---|---|---|---|
| Zee-Babu | $2f_{[ab]}$ | $\mathcal{F}$ | $s_{\{ab\}}$ | $\mathcal{S}$ |
| Type-II seesaw | $\sqrt{2}t_{\{ab\}}$ | $\Delta^\pm$ | $t_{\{ab\}}$ | $\Delta^{\pm\pm}$ |

## IV. EXPLICIT UV COMPLETIONS

### A. Singlet scalars

We consider the ZB model to demonstrate the effects of negative interference and the requirements of reproducing neutrino textures. Using Eqs. (A2) to (A4), we express all of the $f_{ab}$ as a function of only $f_{e\mu}$ and Pontecorvo-Maki-Nakagawa-Sakata matrix data [34]. Note that due to the vanishing $f_{aa}$ couplings of the ZB model, we are now probing nondiagonal couplings. We do this for both the normal and inverted hierarchies, and derive constraints on

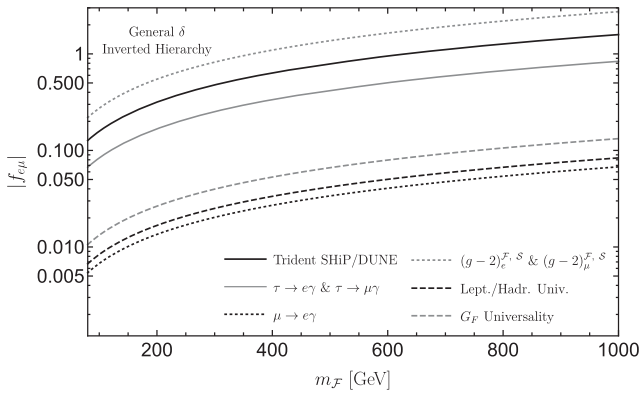


(a) Inverted Hierarchy

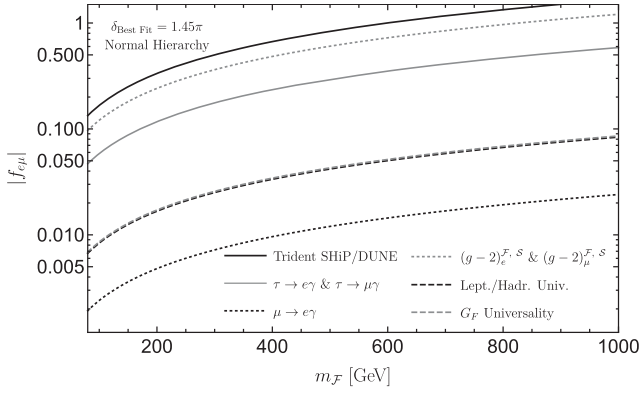


(b) Normal Hierarchy

FIG. 4. Sensitivities for $|f_{e\mu}|$ assuming the Zee-Babu model generates neutrino masses.

$|f_{e\mu}|$ as a function of $m_{\mathcal{F}}$ using the best performing mixed-flavor trident channels. For the normal hierarchy, we set the $CP$-violating phase $\delta$ to its best fit value. For the inverted hierarchy, the dependence on $\delta$ factors out, and so the ZB model's contribution to NTP is independent of $\delta$. Our results are presented in Figs. 4(a) and 4(b).

### B. Triplet scalars: Bounds from CCFR and CHARM-II

The $\nu_\mu \to \nu_i \mu^+ \mu^-$ final state was observed at the CCFR and CHARM-II experiments, and we can calculate experimental bounds on the triplet model using their data. Singlet scalars cannot be probed using this data due to the antisymmetry of the couplings $f_{ab}$.

CHARM-II had a neutrino beam of $\langle E_\nu \rangle \approx 20$ GeV [12,13] with a glass target ($Z = 11$) and the CCFR Collaboration had a neutrino beam of $\langle E_\nu \rangle \approx 160$ GeV using an iron target ($Z = 26$) [12,14]. The two experiments measured production cross sections of [12]

$$\begin{aligned} \sigma_{\text{CHARM-II}}/\sigma_{\text{SM}} &= 1.58 \pm 0.57, \\ \sigma_{\text{CCFR}}/\sigma_{\text{SM}} &= 0.82 \pm 0.28. \end{aligned} \tag{7}$$

Using CCFR as an example, we set bounds by demanding

$$\sigma_{\text{SM+Triplet}} \leq \sigma_{\text{SM}}(0.82 + 1.64 \times 0.28), \tag{8}$$

where 1.64 standard deviations encompasses 90% of a Gaussian likelihood function. For $m_{\mathcal{T}}$ in units of TeV,

$$|t_{\mu\mu}|^2 \left[ \frac{26.38}{m_{\mathcal{T}}^2} + 1.59 \frac{|t_{e\mu}|^2 + |t_{\mu\mu}|^2 + |t_{\tau\mu}|^2}{m_{\mathcal{T}}^4} \right] \leq 691.36 \tag{9}$$

for CHARM-II, and

$$|t_{\mu\mu}|^2 \left[ \frac{34.87}{m_{\mathcal{T}}^2} + 1.97 \frac{|t_{e\mu}|^2 + |t_{\mu\mu}|^2 + |t_{\tau\mu}|^2}{m_{\mathcal{T}}^4} \right] \leq 168.07 \tag{10}$$

for CCFR. Assuming $|t_{ab}| = |t|$, at 90% C.L. the two collaborations impose the following constraints:

$$\begin{aligned} |t| &\leq 3.10 \left( \frac{m_{\mathcal{T}}}{\text{TeV}} \right) \quad \text{CHARM-II}, \\ |t| &\leq 1.77 \left( \frac{m_{\mathcal{T}}}{\text{TeV}} \right) \quad \text{CCFR}. \end{aligned} \tag{11}$$

The stronger bounds from CCFR are a result of the fact that this experiment saw a deficit of events in comparison to the SM prediction and so the upper bound at 90% C.L. is lower than CHARM-II.

## V. CONCLUSIONS AND OUTLOOK

We have investigated NTP as a tool for studying scalar extensions of the SM. We have considered SU(2) singlet, doublet, and triplet charged scalar extensions that couple to leptons, and concluded that triplet and singlet scalar can contribute appreciably to NTP.

In the case of triplet extensions we have found that NTP can serve as a complementary probe of the scalar sector at future experiments. In particular, for specific choices of model parameters in which LFV bounds vanish, NTP provides greater sensitivity than measurements of the anomalous magnetic moment. We found NTP to provide comparable sensitivity for charged singlet scalars and previous $Z'$ models [12] in phenomenologically allowed mass ranges, despite their very different interaction nature. These prospects could be improved as the intensity frontier is pushed forward, and NTP may prove to be a valuable tool in the future. For generic choices of parameters, it is unlikely that NTP can compete with strong LFV constraints.

We have considered both the upcoming experiments SHiP and DUNE. The advantage of DUNE is its ability to isolate beams of $\nu_\mu$ and $\bar{\nu}_\mu$ with high purity by using a magnetic horn. We have shown that this enables us to remove the irreducible background for certain processes, namely $\nu_\mu \to \mu^+ e^- \nu_i$, which has no SM contribution and is a viable production process in triplet models. This has the advantage of providing a clean signal, but results in a sensitivity that scales as $|h|^4$, in contrast to interference effects which can dominate for small coupling and scale as $|h|^2$. The lack of interference with the SM in these particular modes hinders sensitivity. For other channels, the relative phase between the SM and new physics contribution was found to be highly dependent on initial states, which had a tendency to cause destructive (constructive) interference in singlet (triplet) mediated NTP cross sections as can be seen in Appendix C.

The advantages provided by DUNE's nearly monoflavor beam must be balanced against its relatively low-Z detector (argon $Z = 18$) as compared to SHiP (lead $Z = 82$). Additionally DUNE uses a lower energy beam ($\langle E_\nu \rangle = 5$ GeV vs $\langle E_\nu \rangle = 20$ GeV) but compensates for this via a higher number of protons on target. In contrast to DUNE, SHiP's future lead-based detector provides an ideal setting to take advantage of the $Z^2$ coherent enhancement; however the lack of a neutrino horn, and the mutliflavor nature of the neutrino beam, suggests that searches at SHiP will have higher SM irreducible backgrounds.

Lastly, we have investigated representative UV models leading to the generic scalar extensions discussed above. In the ZB and HT models, extra particles and relations between couplings arise if the scalar sector is expected to produce empirically viable neutrino textures. The added constraints due to tree-level lepton flavor violating decays mediated by the doubly charged scalar and from the LHC are especially strong, and in some sense NTP is less important.

The influence of final states on the phase of the SM contribution may be of interest in future applications of NTP to new physics. This dependence is dictated not only

by the flavor combinations in the initial and final states, but also the relative sizes of the charged lepton masses. This final feature is a consequence of the chiral structure of the weak interaction [15]. The influence of these relative phases would be easy to miss and will play a crucial role in any future work that relies on interference with the SM. Although we have considered charged scalars which are already very constrained, we expect many of the qualitative features present in our analysis to be applicable to broader classes of model, in particular, the unique ability of mixed-flavor final states to control the presence or absence of constructive interference. Finally, we were able to identify final mixed-flavor states with no SM counterparts, thus removing irreducible backgrounds. Our results expand the reach of future neutrino experiments—such as DUNE, SHiP, and SBN—to physics beyond their main research program, both within and beyond the SM.

## ACKNOWLEDGMENTS

We are very grateful to Itay Yavin and Maxim Pospelov for their continued guidance and for suggesting mixed-flavor trident production and its potential applicability to scalar models in future intensity frontier experiments. We thank Brian Shuve and Wolfgang Altmannshofer for feedback on the manuscript, as well as Cliff Burgess, Richard Hill, Stefania Gori, Chien-Yi Chen and Sarah Dawson for useful discussions. This research was supported in part by Perimeter Institute for Theoretical Physics. Research at Perimeter Institute is supported by the Government of Canada through the Department of Innovation, Science and Economic Development and by the Province of Ontario through the Ministry of Research and Innovation. This research was also supported by funds from the National Science and Engineering Research Council of Canada (NSERC), and the Ontario Graduate Scholarship (OGS) program.

## APPENDIX A: EXPLICIT UV COMPLETIONS

In what follows we discuss popular implementations of each class of scalar models outlined above. The ZB model, used to radiatively generate neutrino masses, is a representative candidate for singlet scalars $\mathcal{F}$ (see Table I). Two-Higgs-doublet models (2HDM) have been considered extensively in the literature as an implementation of doublets $\mathcal{D}$ and we discuss neutrino trident production's ability to probe their couplings below. Finally the type-II seesaw mechanism (also known as HT models) for the generation of neutrino masses is discussed as the canonical example of a triplet model $\mathcal{T}$.

### 1. Two-Higgs-doublet models

2HDMs have been extensively studied [33,35,36]. In most implementations of a 2HDM there is mixing between the new BSM and SM Higgs doublets. This suggests that for the model to be technically natural couplings between the BSM charged doublet and leptons should be mass weighted to incorporate the influence of the mass-weighted SM Higgs field. In the SM, rates of NTP are log enhanced by infrared phase space effects which are controlled by the small masses of the charged leptons. If one were to consider NTP mediated by the charged component of a doublet scalar extension, this small mass infrared enhancement would compete directly against the mass-weighted Yukawa coupling suppression. Our explicit sensitivity calculations confirm that these competing effects make trident uncompetitive with existing constraints. We note that in the absence of mass-weighted couplings, NTP may be able to address this interesting region of parameter space; however this situation is technically unnatural due to radiative corrections from the Higgs boson—which induces corrections proportional to the SM Yukawa couplings—and would require a new physics mechanism to avoid fine-tuning.

### 2. Zee-Babu model

A popular implementation of the scalar singlet model is the ZB model [6,37,38]. The model features a singly charged scalar $\mathcal{F}$ that couples to the leptonic doublets, and a doubly charged scalar $S$ which couples to the right-handed lepton singlets. The Yukawa sector of the Lagrangian can be written as

$$\begin{aligned}\mathcal{L}_{\mathrm{ZB}} &\supset f_{ab} L_a^i L_b^j \epsilon_{ij} \mathcal{F} + s_{ab} \ell_a^c \ell_b^c \mathcal{S} + \mathrm{H.c.} \\ &= 2 f_{ab} \nu_a \ell_b \mathcal{F} + s_{ab} \ell_a^c \ell_b^c \mathcal{S} + \mathrm{H.c.} \end{aligned} \tag{A1}$$

This model is typically considered in the context of radiatively generated neutrino masses. These first occur at two loops via diagrams such as the one shown in Fig. 5. Assuming the ZB model is fully responsible for the generation of neutrino masses, the mass matrix $M$ can be expressed in terms of the ZB couplings $f_{ab}$ and the SM Yukawa couplings $Y$ via the relation $M \propto fYsY^T f^T$. The antisymmetric matrix $f$ has odd dimensions and therefore its determinant will vanish by Jacobi's theorem. Since the neutrino mass matrix $M$ contains $f$, its determinant will also vanish. This indicates that the smallest neutrino mass $m_1$ ($m_3$) will vanish in the case of the normal (inverted)

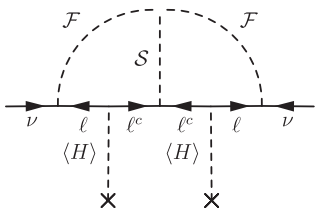


FIG. 5. Neutrino mass generation via the Zee-Babu model using two-component fermions with the direction of the arrows indicating chirality. [23].

hierarchy. The presence of a 0 mass mode [10,39] for the normal hierarchy implies

$$\frac{f_{e\tau}}{f_{\mu\tau}} = \tan\theta_{12}\frac{\cos\theta_{23}}{\cos\theta_{13}} + \tan\theta_{13}\sin\theta_{23}e^{-i\delta}, \quad \text{(A2)}$$

$$\frac{f_{e\mu}}{f_{\mu\tau}} = \tan\theta_{12}\frac{\sin\theta_{23}}{\cos\theta_{13}} - \tan\theta_{13}\cos\theta_{23}e^{-i\delta}, \quad \text{(A3)}$$

and for the inverted hierarchy yields

$$\frac{f_{e\tau}}{f_{\mu\tau}} = -\frac{\sin\theta_{23}}{\tan\theta_{13}}e^{-i\delta}, \qquad \frac{f_{e\mu}}{f_{\mu\tau}} = \frac{\cos\theta_{23}}{\tan\theta_{13}}e^{-i\delta}. \quad \text{(A4)}$$

These relations are used in the results of Sec. IV A, as they provide definite relations between the phases of the various couplings. A phase convention must be chosen, and a simple choice is $0 \leq f_{e\tau} \in \mathbb{R}$. Inspecting Eq. (A4) reveals that if the ZB model is responsible for the observed neutrino textures, and the hierarchy is determined to be inverted, then $0 > f_{e\mu} \in \mathbb{R}$, while $\mathrm{Arg} f_{\mu\tau} = \delta + \pi$. The case of the normal hierarchy is somewhat more involved; however two limits, namely $\delta = 0$ and $\delta = \pi$, result in all the couplings being real and positive by virtue of $\cos\theta_{23} \approx \sin\theta_{23}$ and $\tan\theta_{13} \ll \tan\theta_{12}$.

### 3. Type-II seesaw mechanism

One of the most popular triplet scalar extensions arises in the context of the seesaw mechanism for generating neutrino masses, specifically the so-called type-II seesaw or Higgs triplet model [40–42]. In this version, a triplet field with matrix representation

$$\mathcal{T} \equiv i\sigma_2 \cdot \Delta \equiv -\frac{1}{\sqrt{2}}\begin{pmatrix} -\Delta^0 & \Delta^+ \\ \Delta^+ & \sqrt{2}\Delta^{++} \end{pmatrix} \quad \text{(A5)}$$

is introduced into a symmetric lepton product via an interaction of the form $t_{ab}L_a^i\mathcal{T}_{ij}L_b^j$. After $\Delta^0$ acquires a vacuum expectation value (VEV) $\mathrm{v}_T$, we generate neutrino mass terms of the form $\mathrm{v}_T\nu_a\nu_b t_{ab}$. This model has been ruled out by measurements of the invisible width of the $Z$ boson at LEP [42–44]. These bounds can be evaded by softly breaking the symmetry in the Lagrangian with the terms

$$-m_H^2H^2 + (\mu H^T i\sigma_2\Delta^\dagger H + \text{H.c.}) + M_\Delta^2\mathrm{Tr}(\Delta^\dagger\Delta), \quad \text{(A6)}$$

where $\mu$ can be small to approximately retain the global symmetry. Minimizing this with respect to $\Delta^0$ and setting $\langle\Delta^0\rangle = \mathrm{v}_T$ yields the equation

$$\mathrm{v}_T = \frac{\mathrm{v}_d^2\mu}{\sqrt{2}M_\Delta^2}, \quad \text{(A7)}$$

where $\mathrm{v}_d$ is the SM Higgs' VEV. Since the neutrino masses are given by $\mathrm{v}_T t_{ab}$, we can generate small masses in the limit where $M > \mathrm{v} \equiv \sqrt{\mathrm{v}_d^2 + \mathrm{v}_T^2} = 246$ GeV. As relevant for NTP, we have the Lagrangian

$$\mathcal{L}_{\mathrm{HT}} \supset -t_{ab}\left(\ell^a\Delta^+\sqrt{2}\nu^b + \ell^a\Delta^{++}\ell^b - \frac{\nu^a\Delta^0\nu^b}{\sqrt{2}}\right) + \text{H.c.} \quad \text{(A8)}$$

The flavor symmetry of $t_{ab}$ allows for flavor diagonal terms in the Lagrangian to be nonvanishing. This is in contrast to the singly charged couplings $f_{ab}$ in the ZB model. The off-diagonal flavor couplings with $\Delta^\pm$ can be related to the ZB couplings as shown in Table II. The $\Delta^0$ and $\Delta^{\pm\pm}$ scalars do not contribute to the NTP amplitudes, and so the trident exclusions we obtain on $t_{ab}$ come only from $\Delta^\pm$ leptonic interactions. These must compete with other phenomenological considerations which can be mediated by the $\Delta^{\pm\pm}$ or $\Delta^0$ fields. The propagating degrees of freedom of the scalar sector can, in principle, be different than the fields specified above [40]. However, $\rho$ parameter constraints imply that the triplet VEV is at least 2 orders of magnitude smaller than the Higgs VEV [44]. Therefore the mixing is very small and we can think of $\Delta^\pm$ as being the physical mass eigenstate.

## APPENDIX B: CONSTRAINTS

The addition of charged scalars to the SM leads to a variety of phenomenological consequences. In this section we discuss relevant constraints on the couplings involving the singly charged scalar ($h_{ab}$) and the couplings involving the doubly charged scalar ($k_{ab}$). The latter coupling does not play a role in NTP at tree level; however in the case of a triplet extension bounds on $k_{ab}$ can be converted to constraints on $h_{ab}$ since the two coupling matrices are related to one another as shown in Table II. Below we review existing probes of the scalar sector, which we compare with projected sensitivities using NTP as presented in Sec. IV A.

### 1. Anomalous magnetic moment measurements

Charged scalars can alter a particle's magnetic moment [45–47]. Additionally there is a long-standing discrepancy between the measured value of $(g-2)_\mu$ and the SM prediction [4]. As a result there is some ambiguity in the interpretation of this measurement as either a prediction of the BSM theory or as a constraint on its couplings. These bounds are the weakest of those presented in [10,11]. As shown in Sec. II for certain configurations of parameter space, NTP was capable of exceeding the sensitivity provided by this class of measurements. This is not surprising given NTP's competitive reach in the context of $Z'$ models as outlined in [12].

### 2. Relative decay rates for $\mu$ and $\tau$ leptons

Another class of constraints can be obtained by using the relative size of various measured leptonic decay rates

$$\frac{\Gamma[\tau \to e/\mu + \text{inv.}]}{\Gamma[\mu \to e + \text{inv.}]} \quad \frac{\Gamma[\tau \to \mu + \text{inv.}]}{\Gamma[\tau \to e + \text{inv.}]} \tag{B1}$$

where inv. denotes invisible products (typically neutrinos). Measuring these quantities [48] effectively measures the deviation from unity of flavor ratios of weak couplings $g_W^a/g_W^b$ for various flavors $a$ and $b$. Models with charged scalars generically contribute to $\tau$ decays and so the measurements of Eq. (B1) can be translated as bounds on $||h_{i\tau}|^2 - |h_{ej}|^2|$ as a function of the mass of $h^\pm$ [10]. From the arguments of Ref. [10,28], a singly charged scalar would contribute to the decay $\mu \to e\nu\bar{\nu}$, but would not affect beta decay. Therefore by using data reported in Ref. [48] they were able to constrain $|h_{e\mu}|^2$, by considering a singly charged scalar's contribution to muon decay and noting that only final states with $e\nu_\mu\bar{\nu}_e$ would interfere with the SM amplitude.

The quoted constraint is $|h_{e\mu}|^2 < 0.014(\frac{m_h}{\text{TeV}})^2$ [10] after accounting for the normalizations shown in Table II. The full set of constraints as applied to the ZB model can be found in Tables II and III of Ref. [10], and model independent constraints for a singly charged scalar can be obtained by setting the doubly charged scalar's coupling to 0.

### 3. Loop-level LFV decays

LFV decays of the form $\ell_j \to \ell_i\gamma$ provide another tool to probe $h_{ab}$. This decay mode in the SM is extremely suppressed, and the observation of this LFV process would constitute strong evidence for new physics. Of particular interest is the decay mode $\mu \to e\gamma$ which provides the most stringent constraints on any of the couplings [49].

### 4. Tree-level LFV decays

In the case of triplet extensions where $h_{ab}$ and $k_{ab}$ are necessarily related (as shown in Table II) strong upper limits on certain decay modes [10], such as $\mu^- \to e^+e^-e^-$, already preclude the regions of parameter space trident is capable of probing. On some level these constraints may be evaded by choices related to the Majorana phases in the mass matrix [50,51]; however we have not included these subtleties in our analysis. For singlet scalar extensions $k_{ab}$ and $h_{ab}$ are independent and NTP does not need to compete with bounds related to tree-level LFV decays.

### 5. Implications of the LHC

When including doubly charged scalars, LHC constraints become very strong. There are analyses by both CMS and ATLAS [52,53] on doubly charged scalars decaying to same-sign dileptons which impose a model independent bound on the scalar mass of 200–400 GeV. A recast [54] of these same LHC searches extended the constraints on the mass by an additional 100 GeV by explicitly requiring a total nonzero lepton number in the final state (by considering final states of same-sign dileptons and gauge bosons). Furthermore, Ref. [55] has strengthened this bound by an additional 200 GeV by including recent data from the LHC's most recent 13 TeV run [55].

In Ref. [42], the authors showed that $h \to \gamma\gamma$ measurements at the LHC, the oblique $T$ parameter limits and exclusions from LEP implies a lower bound on $m_{h^\pm}$ as a function of the triplet VEV $v_T$. The VEV enters in the generation of neutrino masses via the relation $M_{ab} = v_T t_{ab}$, as described in Appendix A 3. For example, $v_T \approx 1$ GeV implies $m_{h^\pm} \gtrsim 130$ GeV. This mass constraint gets stronger for lower values of $v_T$. Therefore, the Higgs triplet accounting for neutrino masses has very stringent limits. In the ZB model [10,11], the masses and couplings of the singly and doubly charged scalars can be independently tuned, subject to the constraint that the theory reproduce experimentally viable neutrino textures. There is therefore more flexibility in accommodating current data. In the scenario corresponding to an inverted neutrino mass hierarchy—among other assumptions—the constraints on the doubly charged scalar imply $m_{h^\pm} \geq 200$ GeV.

### 6. Neutrino masses

When considering neutrino masses, there are other sources of constraints that arise in addition to lepton flavor violation. The neutrino mass mixing matrix is related to the scalar triplet's couplings by $m_{ab} = v_T t_{ab}$. Hence, the sensitivity one must achieve in $t_{ab}$ to probe the neutrino mass sector scales inversely with the VEV of the Higgs triplet. This favors using NTP to probe lower values of $v_T$. However, as was discussed in Appendix A 3, this implies a larger $m_{h^\pm}$. Coupled with recent cosmological bounds on the sum of neutrino masses [56], this makes NTP uncompetitive; we have confirmed this fact numerically.

## APPENDIX C: PROJECTED SENSITIVITIES

Given the posterior distribution $P(\theta|\vec{x})$, we can define a 90% C.L. interval [57]. Making use of Bayes' theorem, we can express the posterior probability in terms of a Poisson likelihood, a prior—which is a step function in the signal event rate—and a normalization. The mean of the Poisson distribution is given by $\theta' = B + S$, where $B$ is the background prediction and $S$ is the signal events. Since there is no data $\vec{x}$, we assume that the future experiments will have observed the predicted number of background events. Collecting everything, we have

$$1-\alpha=\int_{-\infty}^{\theta_{\rm up}}P(\theta'|\vec{x})d\theta'=1-\frac{\Gamma(1+B,B+\theta_{\rm up})}{\Gamma(1+B,B)}, \tag{C1}$$

and solve for $\theta_{\rm up}$ given $\alpha=0.1$. Setting $B+\theta_{\rm up}=N_{\rm SM+NP}$, we can set 90% C.L. bounds on the couplings as a function of the masses of the new charged scalars. At SHiP, we take into account backgrounds from incoming $\nu$ and $\bar{\nu}$ whereas at DUNE, we consider only incoming $\nu$. For both collaborations, the signal dependence takes only into account incoming $\nu$. The mass of the new scalar is assumed to be in TeV.

### 1. SU(2) singlet scalar extensions

TABLE III. Projected 90% C.L. sensitivity for a variety of NTP processes mediated by an SU(2) singlet scalar with unit charge at both SHiP and DUNE.

| Final state | SHiP | DUNE near detector |
|---|---|---|
| $e^+\mu^-$ | $17.78\geq\frac{0.62\lvert f_{\mu e}\rvert^2(\lvert f_{e\mu}\rvert^2+\lvert f_{\tau\mu}\rvert^2)}{m_{\mathcal{F}}^4}-\frac{14.47\lvert f_{e\mu}\rvert^2}{m_{\mathcal{F}}^2}$ | $15.53\geq\frac{0.53\lvert f_{\mu e}\rvert^2(\lvert f_{e\mu}\rvert^2+\lvert f_{\tau\mu}\rvert^2)}{m_{\mathcal{F}}^4}-\frac{12.66\lvert f_{e\mu}\rvert^2}{m_{\mathcal{F}}^2}$ |
| $e^+e^-$ | $16.82\geq-\frac{5.56\lvert f_{e\mu}\rvert^2}{m_{\mathcal{F}}^2}+\frac{1.66\lvert f_{\mu e}\rvert^2(\lvert f_{\mu e}\rvert^2+\lvert f_{\tau e}\rvert^2)}{m_{\mathcal{F}}^4}$ | $9.38\geq-\frac{4.48\lvert f_{e\mu}\rvert^2}{m_{\mathcal{F}}^2}+\frac{1.35\lvert f_{\mu e}\rvert^2(\lvert f_{\mu e}\rvert^2+\lvert f_{\tau e}\rvert^2)}{m_{\mathcal{F}}^4}$ |

(C2)

### 2. SU(2) triplet scalar extensions

TABLE IV. Projected 90% C.L. sensitivity for a variety of NTP processes mediated by the singly charged component of an SU(2) triplet scalar field at both SHiP and DUNE.

| Final state | SHiP |
|---|---|
| $e^+\mu^-$ | $17.78\geq\frac{0.04\lvert t_{ee}\rvert^2(\lvert t_{e\mu}\rvert^2+\lvert t_{\mu\mu}\rvert^2+\lvert t_{\tau\mu}\rvert^2)}{m_{\mathcal{T}}^4}+\frac{0.16\lvert t_{\mu e}\rvert^2(\lvert t_{e\mu}\rvert^2+\lvert t_{\mu\mu}\rvert^2+\lvert t_{\tau\mu}\rvert^2)}{m_{\mathcal{T}}^4}+\frac{7.24\lvert t_{e\mu}\rvert^2}{m_{\mathcal{T}}^2}$ |
| $e^+e^-$ | $16.82\geq\frac{0.07\lvert t_{ee}\rvert^2(\lvert t_{ee}\rvert^2+\lvert t_{\mu e}\rvert^2+\lvert t_{\tau e}\rvert^2)}{m_{\mathcal{T}}^4}+\frac{0.42\lvert t_{\mu e}\rvert^2(\lvert t_{ee}\rvert^2+\lvert t_{\mu e}\rvert^2+\lvert t_{\tau e}\rvert^2)}{m_{\mathcal{T}}^4}+\frac{1.23\lvert t_{ee}\rvert^2}{m_{\mathcal{T}}^2}-\frac{2.78\lvert t_{e\mu}\rvert^2}{m_{\mathcal{T}}^2}$ |
| $\mu^+\mu^-$ | $6.43\geq\frac{0.01\lvert t_{e\mu}\rvert^2(\lvert t_{e\mu}\rvert^2+\lvert t_{\mu\mu}\rvert^2+\lvert t_{\tau\mu}\rvert^2)}{m_{\mathcal{T}}^4}+\frac{0.02\lvert t_{\mu\mu}\rvert^2(\lvert t_{e\mu}\rvert^2+\lvert t_{\mu\mu}\rvert^2+\lvert t_{\tau\mu}\rvert^2)}{m_{\mathcal{T}}^4}-\frac{0.04\lvert t_{e\mu}\rvert^2}{m_{\mathcal{T}}^2}+\frac{0.28\lvert t_{\mu\mu}\rvert^2}{m_{\mathcal{T}}^2}$ |
| $\mu^+e^-$ | $11.65\geq\frac{0.02\lvert t_{e\mu}\rvert^2(\lvert t_{ee}\rvert^2+\lvert t_{\mu e}\rvert^2+\lvert t_{\tau e}\rvert^2)}{m_{\mathcal{T}}^4}+\frac{0.07\lvert t_{\mu\mu}\rvert^2(\lvert t_{ee}\rvert^2+\lvert t_{\mu e}\rvert^2+\lvert t_{\tau e}\rvert^2)}{m_{\mathcal{T}}^4}-\frac{0.38\lvert t_{e\mu}\rvert\lvert t_{\mu e}\rvert}{m_{\mathcal{T}}^2}$ |
| Final state | DUNE near detector |
| $e^+\mu^-$ | $15.53\geq\frac{0.13\lvert t_{\mu e}\rvert^2(\lvert t_{e\mu}\rvert^2+\lvert t_{\mu\mu}\rvert^2+\lvert t_{\tau\mu}\rvert^2)}{m_{\mathcal{T}}^4}+\frac{6.33\lvert t_{e\mu}\rvert^2}{m_{\mathcal{T}}^2}$ |
| $e^+e^-$ | $9.38\geq\frac{0.34\lvert t_{\mu e}\rvert^2(\lvert t_{ee}\rvert^2+\lvert t_{\mu e}\rvert^2+\lvert t_{\tau e}\rvert^2)}{m_{\mathcal{T}}^4}+\frac{0.04\lvert t_{ee}\rvert^2}{m_{\mathcal{T}}^2}-\frac{2.24\lvert t_{e\mu}\rvert^2}{m_{\mathcal{T}}^2}$ |
| $\mu^+\mu^-$ | $3.9\geq\frac{0.01\lvert t_{\mu\mu}\rvert^2(\lvert t_{e\mu}\rvert^2+\lvert t_{\mu\mu}\rvert^2+\lvert t_{\tau\mu}\rvert^2)}{m_{\mathcal{T}}^4}+\frac{0.12\lvert t_{\mu\mu}\rvert^2}{m_{\mathcal{T}}^2}$ |
| $\mu^+e^-$ | $2.59\geq\frac{0.06\lvert t_{\mu\mu}\rvert^2(\lvert t_{ee}\rvert^2+\lvert t_{\mu e}\rvert^2+\lvert t_{\tau e}\rvert^2)}{m_{\mathcal{T}}^4}-\frac{0.01\lvert t_{e\mu}\rvert\lvert t_{\mu e}\rvert}{m_{\mathcal{T}}^2}$ |

(C3)


[1] R. Pohl, R. Gilman, G. A. Miller, and K. Pachucki, Muonic hydrogen and the proton radius puzzle, Annu. Rev. Nucl. Part. Sci. **63**, 175 (2013).

[2] R. J. Hill, in Proceedings, 12th Conference on Quark Confinement and the Hadron Spectrum (Confinement XII), Thessaloniki, Greece [*EPJ Web Conf.* 137, 01023 (2017).

[3] F. Jegerlehner and A. Nyffeler, The muon g-2, Phys. Rep. **477**, 1 (2009).

[4] G. W. Bennett *et al.* (Muon g-2 Collaboration), Final report of the muon E821 anomalous magnetic moment measurement at BNL, Phys. Rev. D **73**, 072003 (2006).

[5] A. Aguilar-Arevalo *et al.* (LSND Collaboration), Evidence for neutrino oscillations from the observation of antineutrino (electron) appearance in a antineutrino (muon) beam, Phys. Rev. D **64**, 112007 (2001).

[6] K. S. Babu, Model of calculable Majorana neutrino masses, Phys. Lett. B **203**, 132 (1988).

[7] K. S. Babu and S. Pakvasa, Lepton number violating muon decay and the LSND neutrino anomaly, arXiv:hep-ph/0204236.

[8] M. Lindner, M. Platscher, and F. S. Queiroz, A call for new physics: The muon anomalous magnetic moment and lepton flavor violation, arXiv:1610.06587 [Phys. Rep. (to be published)].

[9] Y.-S. Liu, D. McKeen, and G. A. Miller, Electrophobic Scalar Boson and Muonic Puzzles, Phys. Rev. Lett. **117**, 101801 (2016).

[10] J. Herrero-Garcia, M. Nebot, N. Rius, and A. Santamaria, The Zee-Babu model revisited in the light of new data, Nucl. Phys. **B885**, 542 (2014).

[11] P. S. B. Dev, C. M. Vila, and W. Rodejohann, Naturalness in testable type II seesaw scenarios, Nucl. Phys. **B921**, 436 (2017).

[12] W. Altmannshofer, S. Gori, M. Pospelov, and I. Yavin, Neutrino Trident Production: A Powerful Probe of New Physics with Neutrino Beams, Phys. Rev. Lett. **113**, 091801 (2014).

[13] D. Geiregat *et al.* (CHARM-II Collaboration), First observation of neutrino trident production, Phys. Lett. B **245**, 271 (1990).

[14] S. R. Mishra *et al.* (CCFR Collaboration), Neutrino Tridents and W Z Interference, Phys. Rev. Lett. **66**, 3117 (1991).

[15] G. Magill and R. Plestid, Neutrino trident production at the intensity frontier, Phys. Rev. D **95**, 073004 (2017).

[16] R. Acciarri *et al.* (DUNE Collaboration), Long-Baseline Neutrino Facility (LBNF) and Deep Underground Neutrino Experiment (DUNE), arXiv:1512.06148.

[17] M. Anelli *et al.* (SHiP Collaboration), A facility to Search for Hidden Particles (SHiP) at the CERN SPS, arXiv:1504.04956.

[18] H. Chen *et al.* (MicroBooNE Collaboration), *Proposal for a New Experiment Using the Booster and NuMI Neutrino Beamlines: MicroBooNE* (2007).

[19] R. Belusevic and J. Smith, W-z interference in $\nu$-nucleus scattering, Phys. Rev. D **37**, 2419 (1988).

[20] J. Lovseth and M. Radomiski, Kinematical distributions of neutrino-produced lepton triplets, Phys. Rev. D **3**, 2686 (1971).

[21] R. W. Brown, R. H. Hobbs, J. Smith, and N. Stanko, Intermediate boson. iii. Virtual-boson effects in neutrino trident production, Phys. Rev. D **6**, 3273 (1972).

[22] S.-F. Ge, M. Lindner, and W. Rodejohann, Atmospheric trident production for probing new physics, Phys. Lett. B **772**, 164 (2017).

[23] H. K. Dreiner, H. E. Haber, and S. P. Martin, Two-component spinor techniques and Feynman rules for quantum field theory and supersymmetry, Phys. Rep. **494**, 1 (2010).

[24] V. M. Budnev, I. F. Ginzburg, G. V. Meledin, and V. G. Serbo, The two photon particle production mechanism. Physical problems. Applications. Equivalent photon approximation, Phys. Rep. **15**, 181 (1975).

[25] J. A. M. Vermaseren, New features of FORM, arXiv:math-ph/0010025.

[26] G. Abbiendi *et al.* (LEP, DELPHI, OPAL, ALEPH, L3 Collaborations), Search for charged Higgs bosons: Combined results using LEP data, Eur. Phys. J. C **73**, 2463 (2013).

[27] U. D. Jentschura and V. G. Serbo, Nuclear form factor, validity of the equivalent photon approximation and Coulomb corrections to muon pair production in photon-nucleus and nucleus-nucleus collisions, Eur. Phys. J. C **64**, 309 (2009).

[28] M. Nebot, J. F. Oliver, D. Palao, and A. Santamaria, Prospects for the Zee-Babu Model at the CERN LHC and low energy experiments, Phys. Rev. D **77**, 093013 (2008).

[29] N. Agafonova *et al.* (OPERA Collaboration), Discovery of $\tau$ Neutrino Appearance in the CNGS Neutrino Beam with the OPERA Experiment, Phys. Rev. Lett. **115**, 121802 (2015).

[30] B. J. King *et al.*, Measuring muon momenta with the CCFR neutrino detector, Nucl. Instrum. Methods Phys. Res., Sect. A **302**, 254 (1991).

[31] T. Adams *et al.* (NuTeV Collaboration), Evidence for diffractive charm production in muon-neutrino Fe and antimuon-neutrino Fe scattering at the Tevatron, Phys. Rev. D **61**, 092001 (2000).

[32] A. Buonaura (SHiP Collaboration), *The SHiP experiment and its detector for neutrino physics* (2016).

[33] J. Cao, P. Wan, L. Wu, and J. M. Yang, Lepton-specific two-Higgs doublet model: Experimental constraints and implication on Higgs phenomenology, Phys. Rev. D **80**, 071701 (2009).

[34] I. Esteban, M. C. Gonzalez-Garcia, M. Maltoni, I. Martinez-Soler, and T. Schwetz, Updated fit to three neutrino mixing: Exploring the accelerator-reactor complementarity, J. High Energy Phys. 17 (2017) 87.

[35] T. Abe, R. Sato, and K. Yagyu, Lepton-specific two-Higgs doublet model as a solution of muon g-2 anomaly, J. High Energy Phys. 07 (2015) 064.

[36] G. C. Branco, P. M. Ferreira, L. Lavoura, M. N. Rebelo, M. Sher, and J. P. Silva, Theory and phenomenology of two-Higgs-doublet models, Phys. Rep. **516**, 1 (2012).

[37] T. P. Cheng and L.-F. Li, Neutrino masses, mixings and oscillations in $\mathrm{SU}(2) \times \mathrm{U}(1)$ models of electroweak interactions, Phys. Rev. D **22**, 2860 (1980).

[38] A. Zee, Charged scalar field and quantum number violations, Phys. Lett. **161B**, 141 (1985).

[39] J. Herrero-Garcia, M. Nebot, N. Rius, and A. Santamaria, in Proceedings, 37th International Conference on High Energy Physics (ICHEP 2014), Valencia, Spain, 2014 [*Nucl. Part. Phys. Proc.* 273–275, 1678 (2016)].

[40] P. F. Perez, T. Han, G.-y. Huang, T. Li, and K. Wang, Neutrino masses and the CERN LHC: Testing type-II seesaw, Phys. Rev. D **78**, 015018 (2008).

[41] H. Sugiyama, in *Proceedings, 1st Toyama International Workshop on Higgs as a Probe of New Physics 2013 (HPNP2013), Toyama, Japan, 2013* (2013).

[42] D. Das and A. Santamaria, Updated scalar sector constraints in the Higgs triplet model, Phys. Rev. D **94**, 015015 (2016).

[43] J. C. Montero, C. A. de S. Pires, and V. Pleitez, Spontaneous breaking of a global symmetry in a 331 model, Phys. Rev. D **60**, 115003 (1999).
[44] P. Langacker, *The Standard Model and Beyond, Series in High Energy Physics, Cosmology, and Gravitation* (Taylor and Francis, Boca Raton, FL, 2010).
[45] Y.-L. Wu and Y.-F. Zhou, Muon anomalous magnetic moment in the standard model with two Higgs doublets, Phys. Rev. D **64**, 115018 (2001).
[46] D. A. Dicus, H.-J. He, and J. N. Ng, Neutrino-Lepton Masses, Zee Scalars, and Muon g-2, Phys. Rev. Lett. **87**, 111803 (2001).
[47] C. A. de S. Pires and P. S. Rodrigues da Silva, Scalar scenarios contributing to (g-2)(muon) with enhanced Yukawa couplings, Phys. Rev. D **64**, 117701 (2001).
[48] A. Pich, Precision tau physics, Prog. Part. Nucl. Phys. **75**, 41 (2014).
[49] A. M. Baldini *et al.* (MEG Collaboration), Search for the lepton flavor violating decay $\mu^+ \to e^+\gamma$ with the full data set of the MEG experiment, Eur. Phys. J. C **76**, 434 (2016).
[50] A. Merle and W. Rodejohann, The Elements of the neutrino mass matrix: Allowed ranges and implications of texture zeros, Phys. Rev. D **73**, 073012 (2006).
[51] W. Grimus and P. O. Ludl, Correlations of the elements of the neutrino mass matrix, J. High Energy Phys. 12 (2012) 117.
[52] S. Chatrchyan *et al.* (CMS Collaboration), A search for a doubly charged Higgs boson in $pp$ collisions at $\sqrt{s} = 7$ TeV, Eur. Phys. J. C **72**, 2189 (2012).
[53] G. Aad *et al.* (ATLAS Collaboration), Search for doubly charged Higgs bosons in like-sign dilepton final states at $\sqrt{s} = 7$ TeV with the ATLAS detector, Eur. Phys. J. C **72**, 2244 (2012).
[54] F. del Aguila and M. Chala, LHC bounds on lepton number violation mediated by doubly and singly charged scalars, J. High Energy Phys. 03 (**2014**) 027.
[55] J. Alcaide, M. Chala, and A. Santamaria, LHC signals of radiatively induced neutrino masses and implications for the Zee-Babu model, arXiv:1710.05885.
[56] F. Couchot, S. Henrot-Versillé, O. Perdereau, S. Plaszczynski, B. Rouillé d'Orfeuil, M. Spinelli, and M. Tristram, Cosmological constraints on the neutrino mass including systematic uncertainties, Astron. Astrophys. **606**, A104 (2017).
[57] K. A. Olive *et al.* (Particle Data Group), Review of particle physics, Chin. Phys. C **38**, 090001 (2014).